Statistical selection of the "best" seismic source mechanisms from inversions of synthetic volcanic long-period events

G. S. O'Brien,[1,2] I. Lokmer,[1,2] and C. J. Bean[1,2]

Received 7 September 2009; revised 19 March 2010; accepted 9 April 2010; published 3 September 2010.

[1] Inversions for the source mechanism of long-period (LP) seismicity recorded on volcanoes have become increasingly common and are used to interpret fluid-driven processes. The source mechanism considered for LP inversions usually consists of a symmetric moment tensor with and without single forces. Also, constrained inversions have been performed where one presumes a specific source geometry that reduces the degrees of freedom in the inversion. To select the correct solution from the different possible mechanisms, the Akaike information criterion (AIC) has been used. However, since AIC performs well only if the inverted model is close to the true model, we tested its ability to select the correct model in LP inversions. Using synthetic data sets generated on Mt. Etna, Italy, with a tomography velocity model and the Green's functions calculated for a simplified, homogeneous velocity model, we have investigated (1) if any of the inversion source models can recover the true mechanism and (2) the ability of the Akaike and Bayesian information criteria (BIC) to select the correct model. Results show that in some cases it is possible to recover the mechanism but never the source magnitude and that the BIC is a better measure than the AIC in selecting the true source model, although in numerous cases both criteria fail to select the correct solution. Therefore, the BIC should be used as opposed to the AIC if it is necessary to select an appropriate source. Caution should be used when using the statistical measure in any seismic inversion application.

Citation: O'Brien, G. S., I. Lokmer, and C. J. Bean (2010), Statistical selection of the "best" seismic source mechanisms from inversions of synthetic volcanic long-period events, *J. Geophys. Res.*, *115*, B09303, doi:10.1029/2009JB006958.

1. Introduction

[2] A large class of different seismic events has been observed on active and restless volcanoes. These events span the continuum of observable seismic frequencies and include very long period events (VLP), long-period events (LP), tremor, and tectonic events. VLP and LP events have received particular attention because they have been linked with the volcanic plumbing system as they are thought to be associated with moving fluids or resonating fluid-filled cracks [*Chouet*, 1996; *Neuberg et al.*, 2000]. The frequency bands of VLP and LP events are usually defined in the range ~0.01–0.33 Hz and ~0.33–2 Hz, respectively [*McNutt*, 2005]. Understanding when and how fluids move in a volcanic environment is of paramount importance, hence understanding the source of VLP and LP events is a major aim of volcano seismology. For this reason, inversions for the source mechanisms of these types of sources are becoming increasingly common [e.g., *Ohminato et al.*, 1998; *Chouet et al.*, 2003; *Kumagai et al.*, 2005; 2002; *Nakano et al.*, 2003; *Nakano and Kumagai*, 2005; *Auger et al.*, 2006; *Lokmer et al.*, 2007; *Waite et al.*, 2008]. While the coherency of VLP waveforms is commonly preserved across surveillance networks on volcanoes, LP signals can be distorted by topography and structural heterogeneities [e.g., *Lokmer et al.*, 2007; *Bean et al.*, 2008]. Consequently, inverting for LP sources is a challenging task if the velocity structure is not accurately known (which is, in practice, almost always the case). For example, using eight broadband stations, *Bean et al.* [2008] have shown that the layered nature of the near-surface stratigraphy with strong seismic impedance contrasts can, if not accounted for, leak into the inversion source solution, leading to the emergence of erroneous source geometries, spurious forces, and incorrect source time functions. They suggest constraining the inversions by available geological information and/or increasing the number of the stations deployed in the near-field (as they are less affected by the path effect). However, constraining the source reduces the solution space and prevents us from seeing possible unobserved source properties. With the onset of cheaper broadband seismic stations and larger networks installed on volcanoes, (1) velocity models will improve and (2) the correctness of the solution will improve, even in the case of unconstrained inversions. Therefore, here we analyze constrained and unconstrained LP source inversions using synthetic data "recorded" at a large number of receivers and examine the ability of the Akaike (AIC) and Bayesian information criteria (BIC) to select the model with

[1]School of Geological Sciences, University College Dublin, Dublin, Ireland.
[2]Complex and Adaptive Systems Laboratory, University College Dublin, Dublin, Ireland.

0148-0227/10/2009JB006958

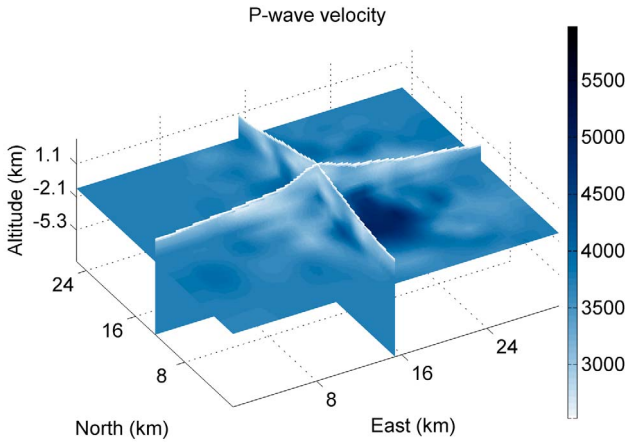

Figure 1. *P* wave velocity structure used to generate the different synthetic data sets. The velocity was taken from the tomography model from the work of *Patané et al.* [2002]. A digital elevation model with a spatial sampling of 40 m of Mt. Etna was used to include the topography.

the minimum number of free parameters required to correctly describe the source mechanism.

[3] When inverting for LP events, the source mechanism is usually considered to consist of a symmetrical moment tensor (six components) with or without single forces (three components). The force terms have been included as LP sources are thought to involve mass transport (of gas and/or liquid). This leads to two different inversions with six and nine free parameters, respectively. If the solution is a priori constrained to be a crack, pipe, explosion, or some other type of source mechanism [see *Nakano and Kumagai*, 2005] the inversion will have less free parameters than an unconstrained inversion, depending on the type of constraints. Since the model with the largest number of free parameters will naturally provide the best fit to the data (but not necessarily a correct solution), a measure for selection of the model with the "correct" number of parameters is required. The Akaike information criterion (AIC) is a commonly used statistical measure to select the "best" model [*Akaike*, 1974]. It has been applied in volcano seismology when inverting VLP and LP signals [*Chouet et al.*, 2003; *Kumagai et al.*, 2005; *Nakano et al.*, 2007; *Ohminato et al.*, 1998]. The model selected by the AIC method has been routinely considered to be the "true" model even though the ability of the AIC to select the correct model depends heavily on the number of data points, the number of free parameters, and the choice of velocity model. In fact, *Akaike* [1974] states that AIC can be used only if the inverted solution is close to the true solution. *Bean et al.* [2008] showed that, in the case of poorly modeled path effects and with only one station in close proximity to the source, the AIC failed to select a correct source model. In this paper, we will extend the work of *Bean et al.* [2008] and examine how AIC performs when source inversions are undertaken using a large number of near-field stations on a model of Mt. Etna volcano. We will invert synthetic LP events for several different possible source models using several different synthetic data sets to examine the robustness of the AIC and the Bayesian information criterion (BIC). The BIC is another statistical measure used for the model selection [*Schwarz*, 1978]. In the following, we will describe the model setup, the synthetic data sets, the inversion techniques, and the statistical measures and then present our results.

2. Synthetic Data Sets

[4] We used elastic full waveform 3-D numerical simulations to generate the synthetic data sets in models of Mt. Etna, Italy. We use an elastic lattice method to model seismic wave propagation in a 3-D elastic medium including complex topography [*O'Brien and Bean*, 2004]. The method is computationally equivalent (in time and memory requirements) to a fourth-order finite difference scheme. For a detailed description of elastic lattice methods and their application to seismic wave propagation, see *Monette and Anderson* [1994] and *O'Brien et al.* [2009]. The *P* wave velocity structure used was taken from the work of *Patané et al.* [2002] and is shown in Figure 1. The model measures 30 km EW, 25 km NS, and 12 km in vertical direction. The tomography model consists of velocities from −1 to 3 km depth, so the synthetic model velocities were extended downward with the bounding velocity at 3 km depth. The surface velocity model was chosen as 1600 m s^{-1}, which linearly increases to the velocity value from the tomography model at −1 km depth. All densities are derived from relationships given by *Corsaro and Pompilio* [2004], and we imposed a Poisson's ratio of 0.25. The spatial resolution was 40 m, and the temporal resolution was 0.008 s. One hundred fifty virtual three-component broadband seismic stations were distributed on the surface to calculate (record) the synthetic data sets. The seismic network is shown in Figure 2 along with a snapshot of the displacement wavefield for a crack source. We generated six different data sets for different source mechanisms where the source function

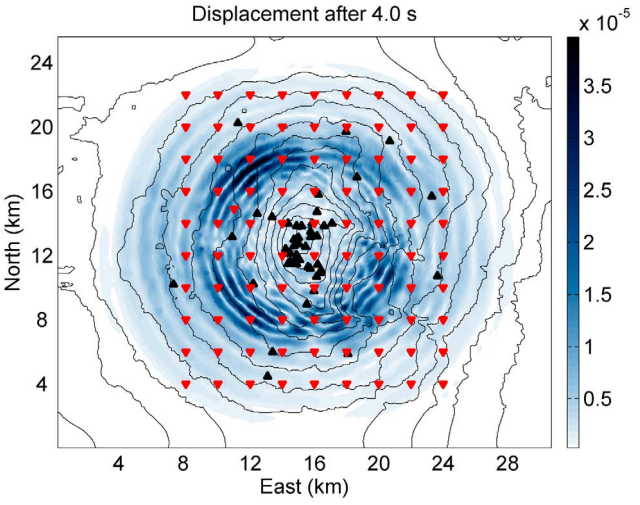

Figure 2. Triangles show the location of the 150 three-component virtual seismometers. The displacement wavefield on the free surface after 4 s for a vertical crack source located 400 m below the summit crater is also shown. The black triangles show the location of the stations for the July 2008 experiment.

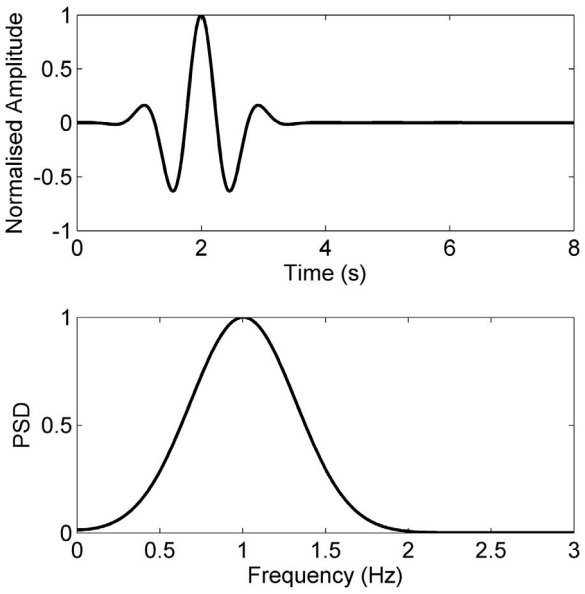

Figure 3. Source wavelet and spectrum used to generate synthetic data sets 1–6 (Table 1).

used in all data sets was a 1 Hz Ricker wavelet (Figure 3). In all cases, we used a shallow source located 400 m below the summit crater. This location and depth corresponds to those of actual LP events recorded on Mt. Etna [*Saccorotti et al.*, 2007]. The source mechanisms for the six different data sets are listed in Table 1. The source mechanisms used represent an isotropic source, isotropic source plus a single vertical force, a vertical pipe, a vertical pipe plus vertical force, a vertical crack oriented in an easterly direction, and vertical E-W crack plus single vertical force. The amplitude of the moment was 1×10^{12} N m and the maximum force amplitude was 2×10^{9} N.

3. Source Models

[5] The observed waveforms u_n can be represented by

$$u_n(t) = M_{pq}(t) \times G_{np,q}(t) + F_p(t) \times G_{np}(t), \tag{1}$$

where M_{pq} is the moment tensor, F_p is a single force, G_{np} are the Green's functions, and n, p, q are the spatial directions. $G_{np,q}$ represents the spatial derivative along the q direction. In the general case, M_{pq} represents the asymmetrical moment tensor (nine components), while F_p is the three-component single force. In this case, the inversion model comprises 12 free parameters. However, since rotational motion is usually not considered in volcano seismicity, we will not include the general asymmetrical moment and restrict the source models to a symmetric moment. If the Green's functions and their derivatives in equation (1), as well as the source location, were perfectly known and if the data set was noise-free, such a general approach would ensure the best possible resolution of the source mechanism properties. However, in practice, one has to deal with the lack of knowledge about the structure and uncertainties in the source location, which can lead to the emergence of spurious moment and force components in the solution. In order to make the solution less prone to these artifacts, the number of free parameters can be reduced by applying certain constraints to a solution model [*Bean et al.*, 2008; *Lokmer et al.*, 2007]. However, in this case, we may not be able to observe some of the source mechanism properties. As suggested by *Bean et al.* [2008], a large number of stations close to the source may improve the resolution and reliability of the inversion solution. Therefore, by using many near-field records for our inversion, we aim to test our ability to select a model with the minimum number of parameters needed to correctly represent the source. Each of the six data sets associated with the six sources described in the previous section will be inverted for 10 source models with different numbers of parameters defined as follows:

$$u_n = \begin{bmatrix} M_o & 0 & 0 \\ 0 & M_o & 0 \\ 0 & 0 & M_o \end{bmatrix} \times G_{np,q} \quad (1 \text{ parameter}), \tag{2}$$

$$u_n = \begin{bmatrix} M_o & 0 & 0 \\ 0 & M_o & 0 \\ 0 & 0 & M_o \end{bmatrix} \times G_{np,q} + \begin{bmatrix} F_x \\ F_y \\ F_z \end{bmatrix} \times G_{np} (4 \text{ parameters}), \tag{3}$$

$$u_n = \begin{bmatrix} 2M_o & 0 & 0 \\ 0 & 2M_o & 0 \\ 0 & 0 & M_o \end{bmatrix} \times G_{np,q} (1 \text{ parameter}), \tag{4}$$

$$u_n = \begin{bmatrix} 2M_o & 0 & 0 \\ 0 & 2M_o & 0 \\ 0 & 0 & M_o \end{bmatrix} \times G_{np,q} + \begin{bmatrix} F_x \\ F_y \\ F_z \end{bmatrix} \times G_{np} (4 \text{ parameters}), \tag{5}$$

Table 1. Description of the Source Mechanisms of the Six Synthetic Data Sets Used in This Study[a]

Data Set	Moment (N m) $[m_{xx}\ m_{yy}\ m_{zz}\ m_{xy}\ m_{xz}\ m_{yz}]$	Force (N) $[F_x\ F_y\ F_z]$	Description
1	M_o[1 1 1 0 0 0]	[0 0 0]	Isotropic
2	M_o[1 1 1 0 0 0]	F_o[0 0 1]	Isotropic + force
3	M_o[2 2 1 0 0 0]	[0 0 0]	Vertical pipe
4	M_o[2 2 1 0 0 0]	F_o [0 0 1]	Vertical pipe + force
5	M_o[3 1 1 0 0 0]	[0 0 0]	E-W crack
6	M_o[3 1 1 0 0 0]	F_o [0 0 1]	E-W crack + force

[a] M_o is 10^{12} N m and F_o is 2×10^{9} N. The source wavelet is shown in Figure 3.

Table 2. Description of the Possible Models Used in the Source Inversions for the Six Synthetic Data Sets

Source Model	Number of Parameters	Moment (N m) $[m_{xx}\ m_{yy}\ m_{zz}\ m_{xy}\ m_{xz}\ m_{yz}]$	Force (N) $[F_x\ F_y\ F_z]$	Description
1	1	M_o[1 1 1 0 0 0]	[0 0 0]	Isotropic
2	4	M_o [1 1 1 0 0 0]	$[F_x\ F_y\ F_z]$	Isotropic + force
3	1	M_o [2 2 1 0 0 0]	[0 0 0]	Vertical pipe
4	4	M_o [2 2 1 0 0 0]	$[F_x\ F_y\ F_z]$	Vertical pipe + force
5	1	M_o [3 1 1 0 0 0]	[0 0 0]	E-W crack 1
6	4	M_o [3 1 1 0 0 0]	$[F_x\ F_y\ F_z]$	E-W crack 1 + force
7	1	M_o [1 3 1 0 0 0]	[0 0 0]	N-S crack 2
8	4	M_o [1 3 1 0 0 0]	$[F_x\ F_y\ F_z]$	N-S crack 2 + force
9	6	$[m_{xx}\ m_{yy}\ m_{zz}\ m_{xy}\ m_{xz}\ m_{yz}]$	[0 0 0]	Moment
10	9	$[m_{xx}\ m_{yy}\ m_{zz}\ m_{xy}\ m_{xz}\ m_{yz}]$	$[F_x\ F_y\ F_z]$	Moment + force

$$u_n = \begin{bmatrix} 3M_o & 0 & 0 \\ 0 & M_o & 0 \\ 0 & 0 & M_o \end{bmatrix} \times G_{np,q}(1\ \text{parameter}), \tag{6}$$

$$u_n = \begin{bmatrix} 3M_o & 0 & 0 \\ 0 & M_o & 0 \\ 0 & 0 & M_o \end{bmatrix} \times G_{np,q} + \begin{bmatrix} F_x \\ F_y \\ F_z \end{bmatrix} \times G_{np}(4\ \text{parameters}), \tag{7}$$

$$u_n = \begin{bmatrix} M_o & 0 & 0 \\ 0 & 3M_o & 0 \\ 0 & 0 & M_o \end{bmatrix} \times G_{np,q}(1\ \text{parameter}), \tag{8}$$

$$u_n = \begin{bmatrix} M_o & 0 & 0 \\ 0 & 3M_o & 0 \\ 0 & 0 & M_o \end{bmatrix} \times G_{np,q} + \begin{bmatrix} F_x \\ F_y \\ F_z \end{bmatrix} \times G_{np}(4\ \text{parameters}), \tag{9}$$

$$u_n = M_{pq} \times G_{np,q}(6\ \text{parameters}), \tag{10}$$

$$u_n = M_{pq} \times G_{np,q} + F_p \times G_{np}(9\ \text{parameters}). \tag{11}$$

All 10 possible source models described by equations (2)–(11) are listed in Table 2. We will refer to the fixed geometry source models (equations (2)–(9)) as constrained inversions as opposed to the unconstrained inversions (equations (10)–(11)) where we invert for all the moment components. We do not invert for the source location but have fixed the location of the source to the true position in all inversions. This implies that we would have a well-constrained source location if we were to use real data.

4. Moment Tensor Inversion

[6] To solve equation (1) for M_{pq} and F_p in an inversion procedure for our six synthetic data sets using the 10 possible source models we need to calculate G_{np}. As we are using synthetic data, we know the exact Green's functions. However, in reality, we do not have access to this information; therefore, we use a homogeneous velocity model with a P wave set to 2300 m s^{-1}. This value was chosen as it is an average of the first 500 m of the true P wave velocity model. The Green's functions are now only an approximation to the true Green's functions. This approximate knowledge replicates a real-world situation where we do not have complete information about the volcano's structure. The spatial derivatives of the Green's functions are calculated from the central finite difference approximation of a spatial derivative with a grid spacing of 40 m. We apply frequency domain inversions to our synthetic seismograms so equation (2) becomes, in the frequency domain,

$$u_n(\omega) = G_{np,q}(\omega) \cdot M_{pq}(\omega) + G_{np}(\omega) \cdot F_p(\omega), \tag{12}$$

where u_n is the nth component of displacement and ω is the frequency. The inversion is performed for each frequency contained in the data, and solutions for M_{pq} and F_p are then transformed into the time domain. The different source inversions are performed by writing equation (12) with the appropriate moment tensor components and single forces. If we form the column vector **d** that contains all the synthetic data components for all the virtual stations, the matrix **G** containing the Green's functions and the derivatives, and column vector **m** containing the moment tensor and single force components, equation (12) can be rewritten in matrix form:

$$\mathbf{d} = \mathbf{G}\mathbf{m}\ . \tag{13}$$

Equation (13) is solved for **m** by minimizing the squared error. The waveform misfit is defined by the residual function R as follows:

$$R = \frac{(\mathbf{d} - \mathbf{G}\mathbf{m})^T(\mathbf{d} - \mathbf{G}\mathbf{m})}{\mathbf{d}^T\mathbf{d}}. \tag{14}$$

On the basis of these residuals and the number of free parameters, AIC and BIC will be calculated for each inverted model.

5. Information Criteria

[7] As the number of free parameters in the inversion increases, the residual defined by equation (14) decreases, i.e., the fit between the model and data improves. Consequently, a model with a large number of free parameters (more than is needed to describe the true solution) will fit the data better than the model with correct number of parameters. In fact, the error in the assumed physical relationship between the model and data (the path effect and the source mislocation in the inversions) and noise contaminating the data will map into the solution in order to improve the fit. The origin of this problem lies in the fact that the residual is estimated based on the data and a model which is derived from the same data set rather than on the data and the true model (that is unknown). This introduces a bias that has to be penalized by a criterion and allows us to select the model with the correct number of parameters for the description of the true solution. If the number of data is relatively small (which is usually the case in seismology), the modified Akaike criterion (AICc) should be used instead of AIC. *Burnham and Anderson* [2002] give an overview of the AIC, and *Kass and Raftery* [1995] describe the BIC and its application. The criteria are defined as follows:

$$\mathrm{AIC} = 2k + n\ln\left(\frac{R}{n}\right), \tag{15}$$

$$\mathrm{AICc} = 2k + n\ln\left(\frac{R}{n}\right) + \frac{2k(k+1)}{n-k-1}, \tag{16}$$

$$\mathrm{BIC} = k\ln(n) + n\ln\left(\frac{R}{n}\right), \tag{17}$$

where k is the number of free parameters plus one, n is the number of data points, and R is the least squares residual given in equation (14). The AIC and AICc are derived from the Kullback-Leibler (K-L) information and the maximized log likelihood where the K-L information can be considered to measure the distance between a model f which is approximated by model g. The additional term in the AICc accounts for a small number of data points relative to the number of free parameters. The right-hand term in equation (16) tends to zero for large n and hence to the AIC. We will only present results using the AICc. The AIC and AICc select the "best" model from the set of considered models with no assumption made about the "truth" of the model. It is not the absolute size of the AIC values but the relative sizes that determine the "best" models with the lowest value pointing to the more likely model. The BIC is founded on Bayesian statistics and asymptotically converges to the true model from a set of possible models as n tends to infinity (in fact, the asymptotic behavior is established quite quickly for small n, so this criterion can be used in practical applications). As with the AIC, the lowest BIC value indicates the "best" model. The BIC penalizes a larger number of free parameters more heavily than the AIC with the natural log of n being the penalizing factor. The choice of using AIC or BIC to select the appropriate model is problem specific with different scenarios giving either the AIC or BIC as the clear winner [*Burnham and Anderson*, 2002; *Kass and Raftery*, 1995]. In simple terms, the BIC selects a simpler model (less free parameters) than the AIC. It must be stressed that these measures are only valid when comparing the same data set (i.e., the same seismograms) and they do not discount models but merely indicate the more likely solution. As we are performing the inversion in the frequency domain, the value of k and n are given by

$$k = (\text{number of free parameters} + 1)N_{\mathrm{f}}, \tag{18}$$

$$n = (\text{number of free seismograms})N_{\mathrm{f}}, \tag{19}$$

where N_{f} is the number of nonzero frequency terms in the Fourier transform of the seismograms. In a practical situation using a fast Fourier transform and computational methods, there are no zero frequency terms, so N_{f} is determined by the frequency interval of interest, which, for the 1 Hz Ricker wavelet used in this study, was chosen as 0–3 Hz. If we use all the frequencies in the Fourier transform, the residuals do not change sufficiently to alter the results. For our six data sets, we inverted for the 10 possible source models for different numbers of stations in different station distributions and examined the ability of the inversion to recover the source mechanism and the ability of the AICc and BIC to select the correct source model.

6. Inversion Results

[8] To test the consistency of the numerical methods for the wave propagation, Green's function calculations, their derivative approximations, and the inversion codes, we inverted for synthetic data sets, which were generated using the homogenous velocity model. As Green's functions are also calculated in a homogenous velocity model, they are now exact; hence, the only error in the inversion is our ability to accurately sample the wavefield. The ability to adequately sample the wavefield depends nontrivially on the complexity of the velocity model, the source radiation pattern, the number of stations, and the station distribution. Ten stations, chosen at random from the 150 possible stations, are sufficient to recover the true solution for a perfectly known velocity model. For each of the different source models, the statistical measures, AICc and BIC, clearly distinguish the correct choice. The reconstruction of the source mechanism and the ability of the statistical measures to select the correct model when more than 10 stations are used is of no great surprise as the Green's functions are exact and there are no errors (except for numerical approximations) in the solution.

[9] The situation is quite different when we invert for data sets 1–6 (calculated for a heterogeneous velocity model) using different numbers of stations with different station distributions. Figure 4 shows an example of one station distribution consisting of 25 stations selected at random from the possible 150 stations. The comparison of the synthetic seismic traces from data set 1 (isotropic source) and the inversion-derived seismograms for source models 1 and 10 are shown in Figures 5 and 6, respectively. The

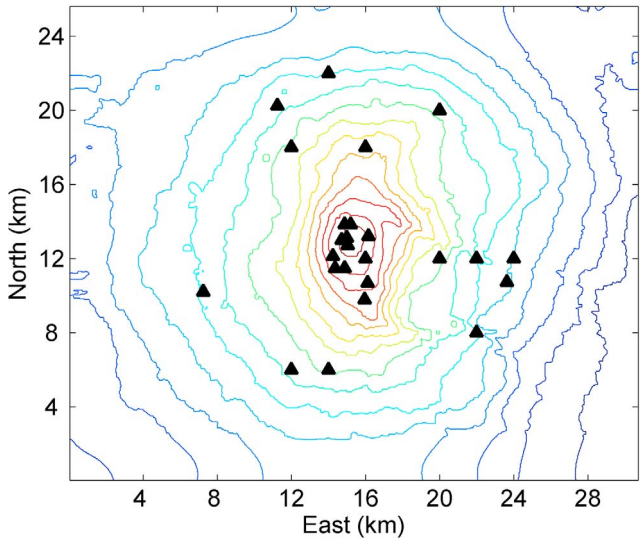

Figure 4. Triangles show one distribution of the 25 stations used to invert for data set 1 for 10 possible source models (Table 2). The stations are chosen at random from the possible 150 stations in Figure 2. The results of the inversion of this particular station distribution are shown in Figures 7–9.

seismograms are normalized to the maximum amplitude at the station closest to the source and are labeled from 1 to 25 with increasing distance from the source. It can be seen that model 10 provides a better fit for the near-field stations even though model 1 is the correct model. This is to be expected as we have increased the number of free parameters from 1 to 9. The source mechanism recovered for each of the 10 possible models is shown in Figures 7, 8, and 9. All the source models cannot recover the true moment magnitude as the compliance of the tomography model and Green's function homogeneous model differs hence the magnitude differs. The correct source mechanism is recovered only for model 1 (by definition) and approximately by model 9 though the source time function and amplitudes are wrong. There is also some small amplitude nonzero off diagonal components in this solution, which should not exist. In all other cases, we have nonzero single forces and an incorrect moment. Changing the random station distribution does not significantly affect the generic pattern of the inversion results. When we increase the number of stations to 50, the solution improves for all different station distributions chosen at random. Models 1 and 9 again provide the correct solution. When single forces are included in the possible sources, a strong vertical force is present in all cases. As for 25 stations, for 50 stations, all source models do not recover the correct source magnitude. Increasing the number of stations to 100 does not dramatically improve the solution. Figures 10, 11, and 12 show the results of inverting data set 5 (vertical crack with no force terms) for one distribution of 25 stations selected at random from the 150 possible stations. Source model 5 is by definition the correct model and hence provides an adequate solution save for the source magnitude. Source models 9–10 could provide a correct solution but fail to do so as the errors in the Green's functions mask the true solution.

[10] The AICc and BIC were calculated for numerous different station distributions comprising 10, 25, 50, and 100 stations. Again, it should be noted that the AICc and BIC should not be compared for different data sets only among the different source models for the same data set, i.e., each different station distribution should be viewed independently. The results along with the misfit residuals are shown in Figures 13 and 14. For 10 stations, a large scatter is seen between different station distributions. The large scatter for a small number of stations is expected as the station distribution is very important in resolving the radiation pattern. In the case of the five examples shown in Figure 13 using 10 stations, the dispersion of errors is similar. In this case, the examples selected at random have a large number of far-field stations therefore even though the actual details of the inversion differ significantly the errors and statistical measures are similar. With only 10 stations chosen at random, we can select at random only far-field stations or a distribution with a poor azimuthal coverage leading to a poor inversion and large misfits. In a real-world scenario, one would avoid selecting 10 station locations at random and especially in the far field. For all inversions (with 25 or more stations), it is clearly seen that the models including the single forces (even number models) are the

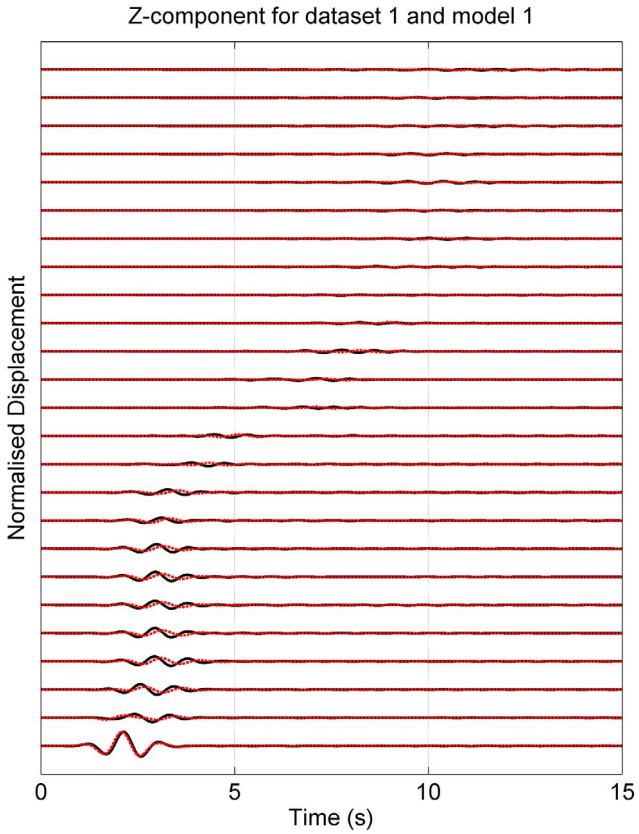

Figure 5. Twenty-five vertical component synthetic seismograms (solid lines) from data set 1 and the resultant seismograms from an inversion assuming an isotropic point source, model 1 (dashed lines). The seismograms are shown from bottom to top with increasing distance from the source and are normalized to the closest station. The station locations are shown in Figure 4.

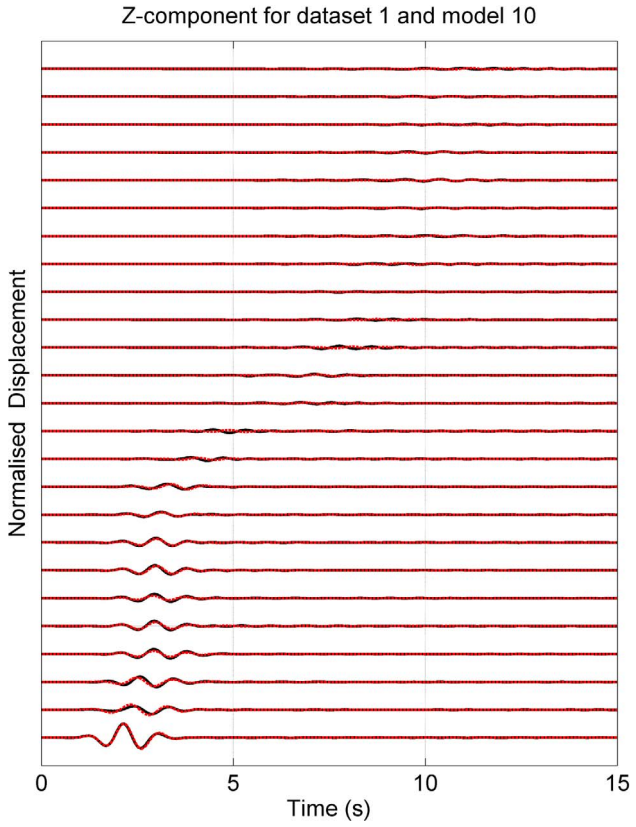

Figure 6. Twenty-five vertical component synthetic seismograms (solid lines) from data set 1 and the resultant seismograms from an inversion assuming a symmetric moment tensor and single forces, source model 10 (dashed lines). The seismograms are shown from bottom to top with increasing distance from the source and are normalized to the closest station. The station locations are shown in Figure 4.

"best" models even though the single forces are not included in this data set. The *P* wave radiation pattern of a vertical force is similar to an isotropic source when viewed from the volcano's surface, and hence, as we are restricted to sampling on the surface, the vertical force provides a reasonable solution when coupled with the error associated with the approximate Green's functions. When we invert for data set 2, where we have an isotropic source and single vertical force, and examine the AICc and BIC for five different station distributions comprising of 50 and 100 stations, we see a similar result for data set 1. In all cases, the model including single forces is clearly the better model and both the AICc and BIC select the correct models 2 and 10 as the best solution (Figure 15) (model 10 results in an isotropic moment tensor).

[11] Figures 13–15 show distributions of the residual, AICc, and BIC from five inversions out of a total of 500 using different numbers of stations and are shown to illustrate the variation in the AICc and BIC values. For every inversion, the source model with the lowest AICc or BIC value is regarded as the best solution. Figures 16 and 17 show a histogram of the number of source models with the minimum AICc and BIC value for all 500 inversions

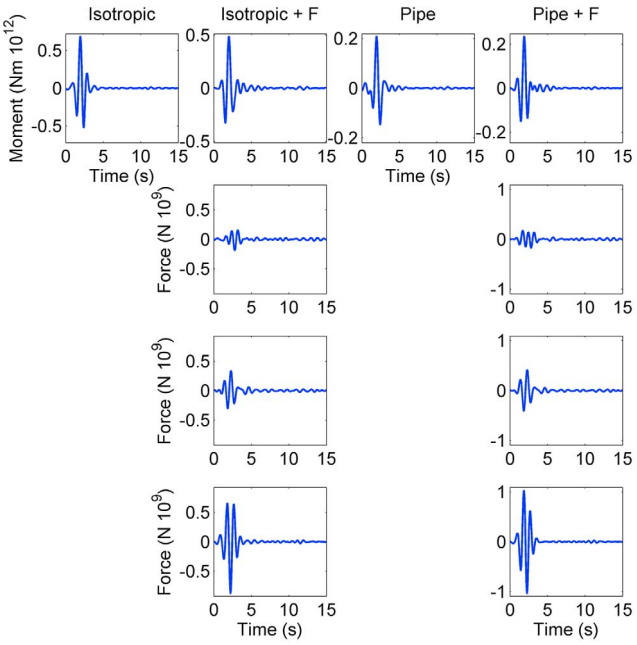

Figure 7. Inversion results for source models 1–4 for data set 1 (isotropic source) for the station distribution shown in Figure 4. The actual seismograms and resultant inversion fitted seismograms are shown in Figure 5 for the isotropic source. The amplitude of the source moment was 10^{12} N m. For the source models without forces, there is only one independent component, and for the others, there are four free parameters.

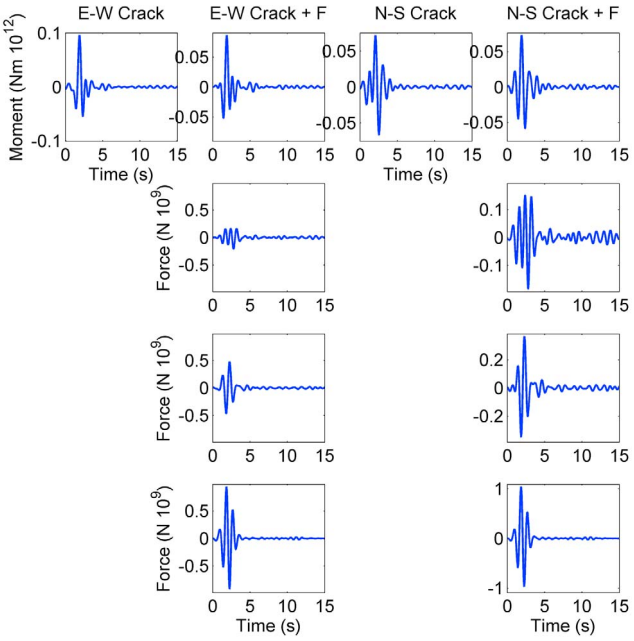

Figure 8. Inversion results for source models 5–8 for data set 1 (isotropic source) for the station distribution shown in Figure 5. The amplitude of the source moment was 10^{12} N m. For the source models without forces, there is only one independent component, and for the others, there are four free parameters.

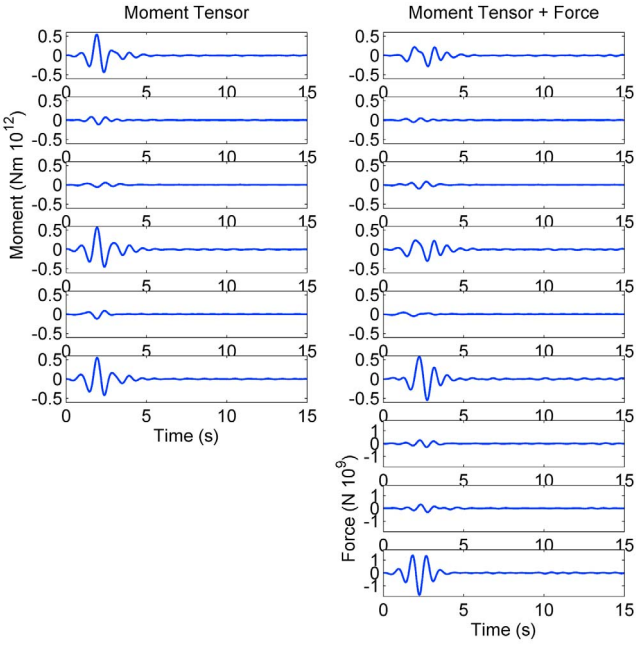

Figure 9. Inversion results for source models 9–10 for data set 1 (isotropic source) for the station distribution shown in Figure 4. The actual seismograms and resultant inversion fitted seismograms are shown in Figure 6 for the moment and single forces. The moments and force components are arranged as $[m_{xx}\ m_{xy}\ m_{xz}\ m_{yy}\ m_{yz}\ m_{zz}]$ and $[F_x\ F_y\ F_z]$ from top to bottom. The amplitude of the source moment was 10^{12} N m.

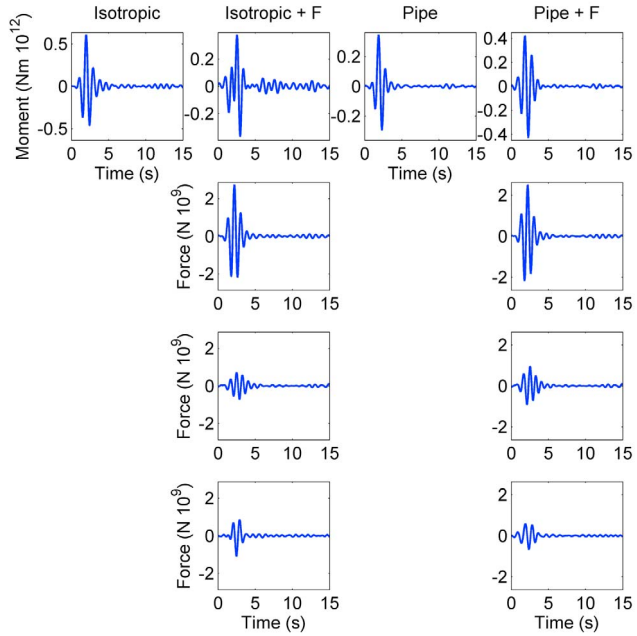

Figure 10. Inversion results for source models 1–4 for data set 5 (crack source) for 50 stations selected at random from the possible 150. The amplitude of the moment was 10^{12} N m.

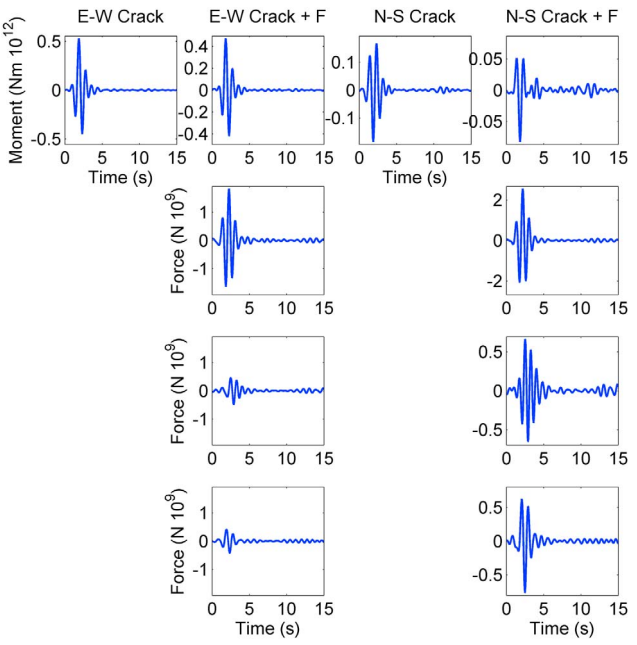

Figure 11. Inversion results for source models 5–8 for data set 5 (crack source) for the same 50 stations selected at random as in Figure 10. The amplitude of the moment was 10^{12} N m.

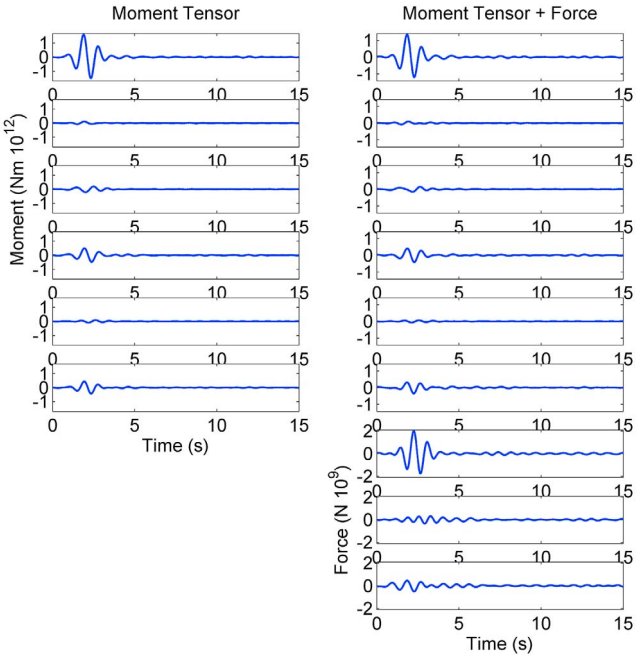

Figure 12. Inversion results for source models 9–10 for data set 5 (crack source) for the same 50 stations selected at random as in Figure 10. The moments and force components are arranged as $[m_{xx}\ m_{xy}\ m_{xz}\ m_{yy}\ m_{yz}\ m_{zz}]$ and $[F_x\ F_y\ F_z]$ from top to bottom. The amplitude of the moment was 10^{12} N m.

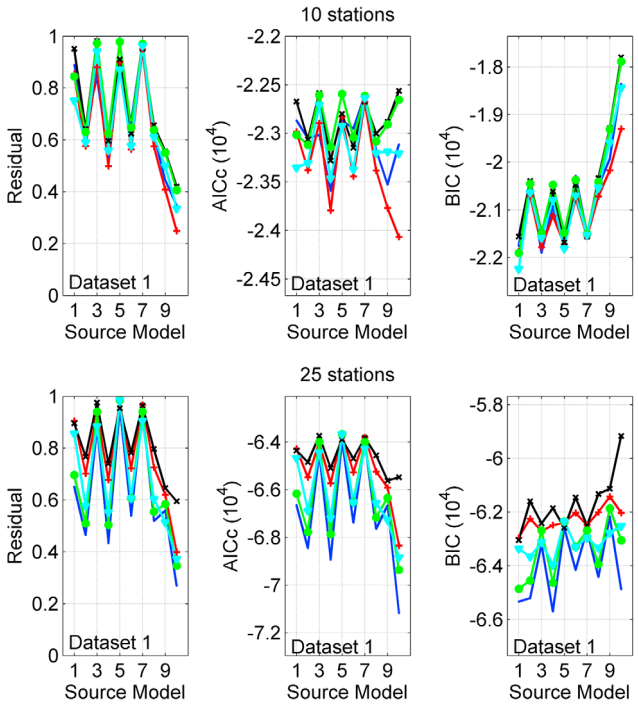

Figure 13. Residuals, AICc, and BIC calculated for five different station distributions (represented by different symbols) for all 10 possible source models for data set 1. (top) Distributions of 10 stations. (bottom) Distributions of 25 stations. The true solution is model 1 and can be source model 9. The lowest AICc and BIC value indicates the "best" model.

using 50 stations. Source model 10 is consistently chosen as the best model for all data sets using the AICc value. The BIC value is more variable selecting different possible source models for different data sets. For data sets 2, 4, 5, and 6, the BIC has a reasonable success rate in selecting the correct model. For every inversion, we examined if source model 10 provided the correct solution. The moment and force normalized amplitudes (relative to M_{xx}) are shown in Figure 18. For the solution to be correct, the amplitudes of each component should fall within the solid circles. For each data set, a large single vertical force is observed leading to an erroneous solution. Therefore, the AICc consistently fails to select the correct model as the penalizing term for a larger number of free parameters is not severe enough. The BIC provides a more robust measure of the correct solution but is heavily dependent on the station distribution. We observed similar results for distributions using 100 stations. For inversions of 25 stations, the AICc again consistently selected source model 10 while we observed a larger variation of the BIC best model.

[12] Having 150 broadband stations on a volcano would represent an ideal scenario. In reality, we are generally restricted to a smaller number of stations with restrictions on a desired uniform station distribution due to access and safety constraints. To investigate the accuracy of the inversion and the ability to determine the correct source model in a real-world scenario, we have inverted all six synthetic data sets using a station distribution (52 stations) taken from a seismic experiment carried out on Mt. Etna in July 2008 (see Figure 2), *De Barros et al.* [2009] discuss the results of this experiment. In this case, we have a densely populated network close to the source epicenter with a gap on the eastern flank due to the inaccessibility of Valle del Bove. Five hundred inversions were performed where we selected 15 stations at random from the possible 52. The source model selected by the AICc and BIC for these inversions is shown in Figures 19 and 20. As with the previous cases, the AICc selects source model 10 for the vast majority of the different station distributions. The solution from source model 10 is shown in Figure 21 and clearly illustrates that the AICc fails to select the correct mechanism. The single forces are large, and a large variation is observed for M_{zz}. The BIC has more success in selecting the correct source from the constrained inversions; however, the station distribution plays a major role in determining the ability to accurately select the correct model. A tightly packed station distribution with a good azimuthal coverage provides the best results. We also inverted the six synthetic data sets for the 10 source models and calculated the AICc and BIC measures for all 52 stations (Figure 22). This would represent a best case scenario. If we examine the data sets with no vertical force, we see that the AICc does not select the correct model in all three cases. The BIC is successful in selecting only the correct model for a pipe source. The correct model is highlighted by a vertical line in Figure 22.

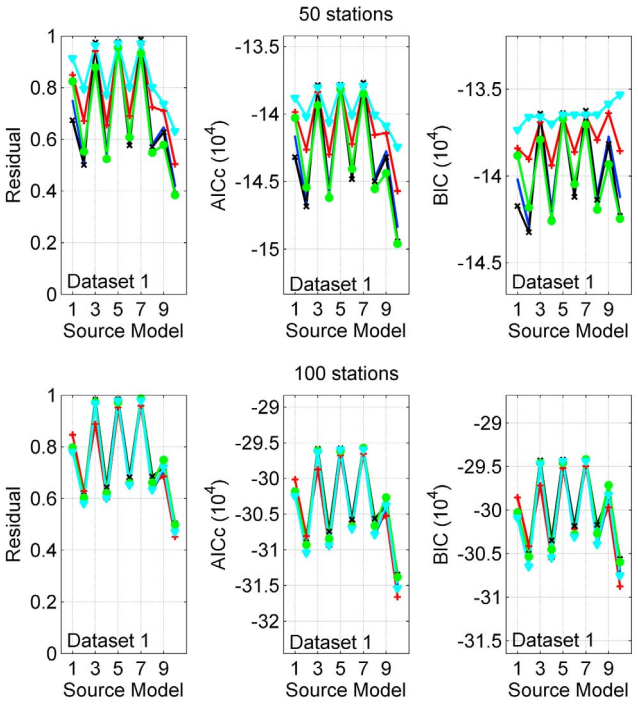

Figure 14. Residuals, AICc, and BIC calculated for five different station distributions (represented by different symbols) for all 10 possible source models for data set 1. (top) Distributions of 50 stations. (bottom) Distributions of 100 stations. The true solution is model 1 and can also be source model 9.

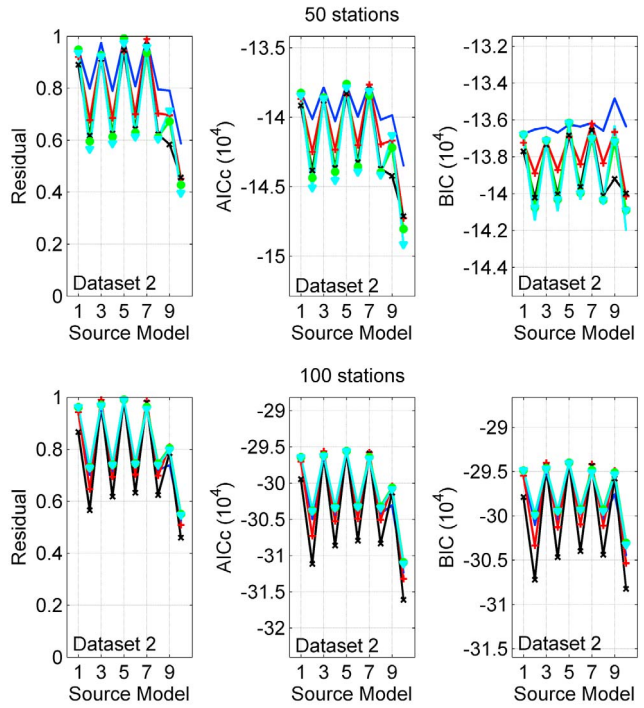

Figure 15. Residuals, AICc, and BIC calculated for five different station distributions (represented by different symbols) for all 10 possible source models for data set 2. (top) Distributions of 50 stations. (bottom) Distributions of 100 stations. The true solution is model 2 and can be source model 10.

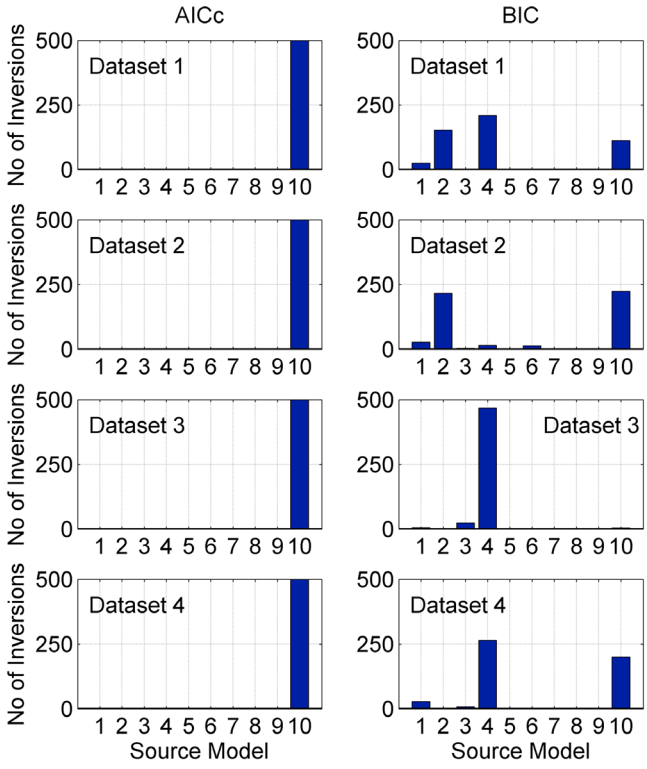

Figure 16. Source models selected by the AICc and BIC for 500 inversions of 50 stations each are shown for data sets 1–4.

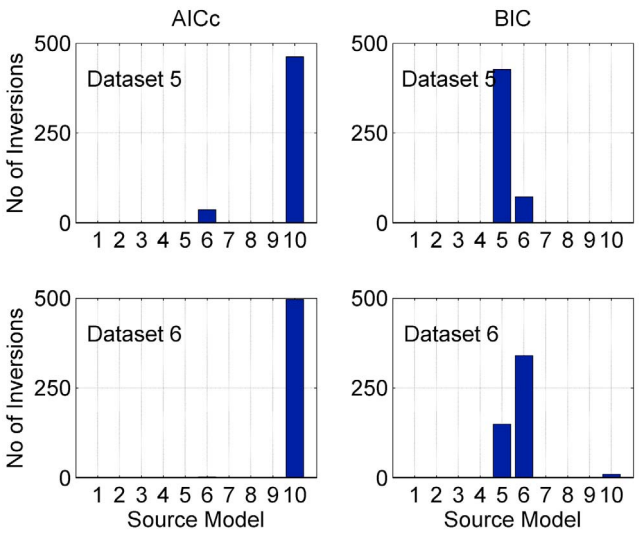

Figure 17. Source models selected by the AICc and BIC for 500 inversions of 50 stations each are shown for data sets 5 and 6.

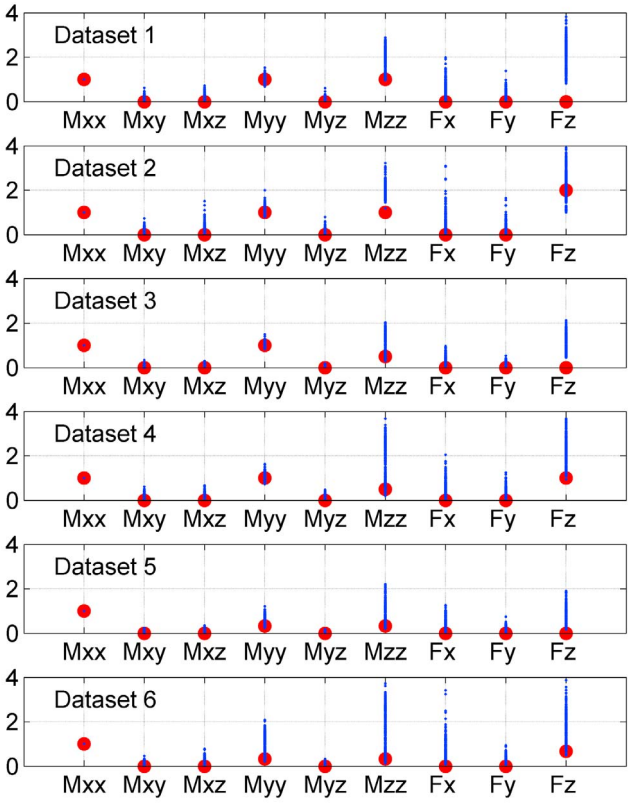

Figure 18. The normalized moment and force amplitudes from source model 10 are shown as dots. The 500 inversions are for 50 stations selected at random from the possible 150. The moments are normalized relative to M_{xx}. The single forces were normalized with respect to $M_{xx}/1000$. The source mechanism for each data set is shown as the large circles. For the solution to be correct, the dots should lie within the circles. It can be seen from the large vertical forces that source model 10 cannot recover the true solution.

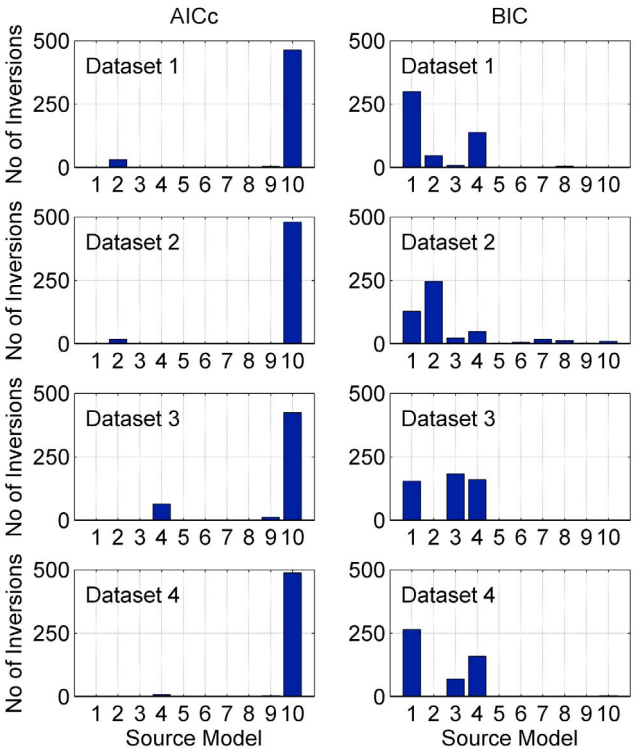

Figure 19. Source models selected by the AICc and BIC for 500 inversions of 15 stations selected at random for the July 2008 locations each are shown for data sets 1–4.

When single forces are included, both measures fail to select the correct model. The only way that the AICc and BIC can select the true model is if we were not to include the unconstrained inversions. Then both measures select the correct model for data sets 2, 4, and 6. As with the previous examples, we cannot recover the magnitude of either the moment tensor or the single forces even when the statistical measures select the correct model. This results from a lack of knowledge of the highly compliant near-surface structure.

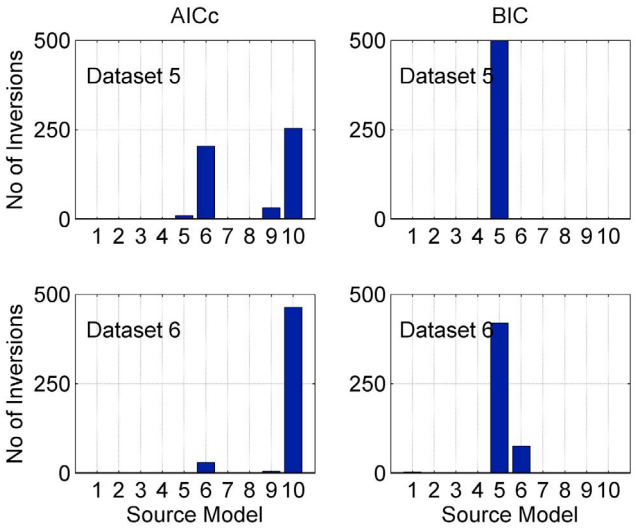

Figure 20. Source models selected by the AICc and BIC for 500 inversions of 15 stations selected at random for the July 2008 locations each are shown for data sets 5 and 6.

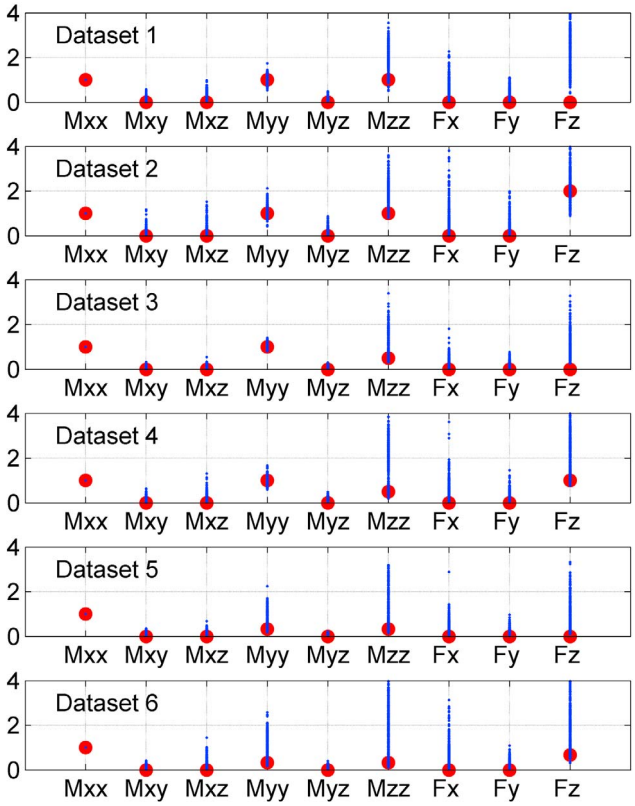

Figure 21. The normalized moment and force amplitudes from source model 10 are shown as dots. The 500 inversions are for 15 stations selected at random form the 52 possible locations from the July 2008 experiment. The moments are normalized relative to M_{xx}. The single forces were normalized with respect to $M_{xx}/1000$. The source mechanism for each data set is shown as the large circles. For the solution to be correct, the dots should lie within the circles. It can be seen from the large vertical forces that source model 10 cannot recover the true solution.

7. Discussion and Conclusions

[13] We use 3-D full wavefield numerical simulations, a realistic volcano-seismic source mechanism and topography of Mt. Etna to examine the validity of using the AICc and/or the BIC to identify the correct seismic source model from several possible contenders. To replicate the lack of knowledge of a volcano velocity structure, we have generated synthetic data sets using a tomography-derived velocity model and generated our Green's functions, which are used in the inversion procedure, using a homogenous velocity structure. This was done to replicate a situation where we do not have complete knowledge of the real velocity structure and thus will introduce errors into the Green's functions. This will then introduce errors into the inversion results as would be expected when inverting for real data. The errors associated with the approximate Green's functions depend on the frequency of the LP events under consideration. We also generated the six data sets for a source with a central

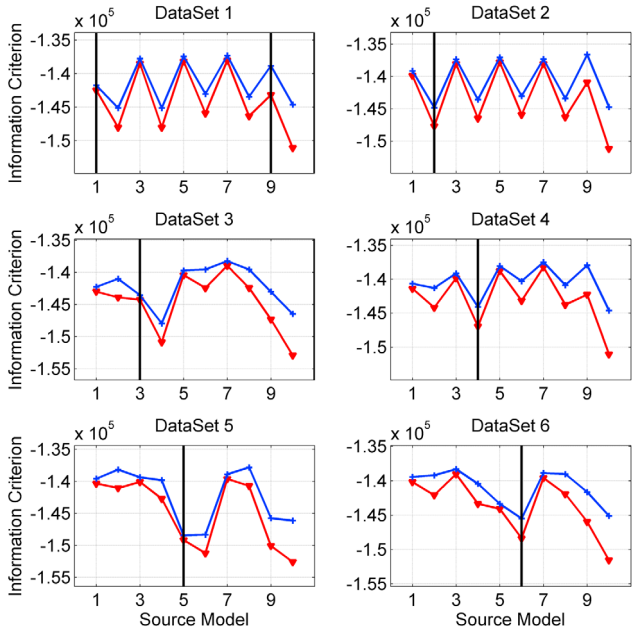

Figure 22. AICc (triangles) and BIC (crosses) values calculated from the residuals from an inversion of all 52 stations from the July 2008 experiment. The solid lines show the true solution.

frequency of 0.4 Hz and found that the results presented for 1 Hz are applicable to these lower-frequency synthetic data sets. We have fixed the location of the source to the true position in all inversions, which implies that we would have a well-constrained source location if we were to use real data. If we were to allow the source location to be included into the inversion procedure, we would hugely increase the degrees of freedom in the problem and would effectively use the variable source position to minimize the errors introduced by using approximate Green's functions. We have also restricted our source models to specific source mechanisms (i.e., a vertically oriented crack with an east normal and a vertical pipe). Following the procedure of *Nakano and Kumagai* [2005], we could have searched for the orientation of these geometries. We did run initial tests using this methodology and found that the lowest residuals for the crack and pipe structures were always within 10° of the true structure and did not significantly alter our results. Therefore, to minimize the number of inversions (>5000) and hence the computational time, we fixed the crack and pipe orientations.

[14] For all inversions for all source models, we could not recover the correct amplitude for the moment tensor and single forces components. A maximum difference of 1 order of magnitude was observed. This value will depend on the discrepancy between the compliance of the volcano edifice and the model used to generate the Green's functions. Therefore, caution should be exercised when extracting any information about the magnitude of volume changes and the associated consequences for volcanic fluids. When the number of stations is low (<10–25), the ability to accurately recover the source mechanism depends heavily on the station distribution with different distributions giving significantly different solutions. This variability is also reflected in the AICc's and BIC's inability to consistently select the correct model. A densely well-distributed network provides the best results by adequately sampling the wavefield. This result is consistent with the synthetic results from *Bean et al.* [2008]. When the number of stations in the station distribution increases, the solutions converge to a single solution independent of the particular network. In this case, the wavefield is adequately sampled to recover the source and any misfit can be attributed to the approximate Green's functions. For the unconstrained inversions, this approximation leaks into the solution and leads to the wrong source mechanism for all data sets except for an isotropic and pipe source mechanism without single forces. When it is applicable, the constrained inversion (solving for a specific, arbitrarily oriented source mechanism) provides the more reliable results. The ability of the AICc and BIC to select the true model from the 10 possible source models depends on the number of stations used in the inversions and on whether single forces are included in the data set or not. The AICc consistently fails to select the correct model and is a poor indication of the "best" source model. The BIC is a more reliable indicator of the true solution but still can select the wrong model. It converges to the "true" solution asymptotically as the number of data tends to infinity; it performs best when there is a large number of stations. The number of stations needed depends on the complexity of the source model, i.e., the number of free parameters needed to fully describe the source. The accuracy of the AICc selection does not increase with increasing number of stations. If we restrict our inversions to constrained solutions, both the AICc and BIC perform well. The AICc preferentially selects the unconstrained solution regardless of whether they are close to the true source as the number of free parameters is not penalized severely enough. Therefore, we conclude from our synthetic tests and from the discussion of *Bean et al.* [2008] that when inverting for LP events it is best to use as much a priori information to constrain the possible source models and to minimize the errors associated with approximate calculations of the Green's functions. Finally, to differentiate between these possible seismic source models, the BIC is a more reliable measure of the validity of the "best" source models than the AICc, but caution must be exercised in applying the BIC. To aid in the interpretation of the BIC results, numerical tests on multiple synthetic data sets can be used to quantify the accuracy of this measure for the specific problem under consideration.

[15] **Acknowledgments.** The authors wish to acknowledge that this work was carried out in part by the Department of Communications, Energy and Natural Resources under the National Geoscience Programme 2007–2013 and the SFI RFP 2007 award. The SFI/HEA Irish Centre for High-End Computing (ICHEC) is acknowledged for the provision of computational facilities and support. Discussion with B. Murphy about the statistical implications was greatly appreciated. The authors wish to thank Javier Almendros, an anonymous reviewer, and the Associate Editor for their constructive comments that improved the manuscript.

References

Akaike, H. (1974), A new look at the statistical model identification, *IEEE Trans. Autom. Control*, *19*, 716–723, doi:10.1109/TAC.1974.1100705.

Auger, E., L. D'Auria, M. Martini, B. Chouet, and P. Dawson (2006), Real-time monitoring and massive inversion of source parameters of very

long period seismic signals: An application to Stromboli Volcano, Italy, *Geophys. Res. Lett.*, *33*, L04301, doi:10.1029/2005GL024703.

Bean, C. J., I. Lokmer, and G. S. O'Brien (2008), The influence of near-surface volcanic structure on long-period (LP) seismic signals and source inversions: Simulated examples from Mt. Etna, *J. Geophys. Res.*, *113*, B08308, doi:10.1029/2007JB005468.

Burnham, K. P., and D. R. Anderson (2002), *Model Selection and Multi-Model Inference: A Practical Information-Theoretic Approach*, 2nd ed., 488 pp., Springer, New York.

Chouet, B. (1996), Long-period volcano seismicity: Its source and use in eruption forecasting, *Nature*, *380*, 309–316, doi:10.1038/380309a0.

Chouet, B. A., P. Dawson, T. Ohminato, M. Martini, G. Saccorotti, F. Giudicepietro, G. D. Luca, G. Milana, and R. Scarpa (2003), Source mechanisms of explosions at Stromboli Volcano, Italy, determined from moment-tensor inversions of very long period data, *J. Geophys. Res.*, *108*(B1), 2019, doi:10.1029/2002JB001919.

Corsaro, R. A., and M. Pompilio (2004), Buoyancy of magmas at Mt. Etna, *Terra Nova*, *16*, 6–22.

De Barros, L., C. J. Bean, I. Lokmer, G. Saccorotti, L. Zuccarello, G. S. O'Brien, J. P. Metaxian, and D. Patane (2009), Source geometry from exceptionally high resolution long period event observations at Mt. Etna during the 2008 eruption, *Geophys. Res. Lett.*, *36*, L24305, doi:10.1029/2009GL041273.

Kass, R. E., and A. E. Raftery (1995), Bayes Factors, *J. Am. Stat. Assoc.*, *90*, 773–795, doi:10.2307/2291091.

Kumagai, H., B. Chouet, and M. Nakano (2002), Waveform inversion of oscillatory signatures in long-period events beneath volcanoes, *J. Geophys. Res.*, *107*(B11), 2301, doi:10.1029/2001JB001704.

Kumagai, H., B. Chouet, and P. Dawson (2005), Source process of long-period event at Kilauea volcano, Hawaii, *Geophys. J. Int.*, *161*, 243–254, doi:10.1111/j.1365-246X.2005.02502.x.

Lokmer, I., C. J. Bean, G. Saccorotti, and D. Patanè (2007), Moment-tensor inversion of LP events recorded on Etna in 2004 using constraints obtained from wave simulation tests, *Geophys. Res. Lett.*, *34*, L22316, doi:10.1029/2007GL031902.

McNutt, S. (2005), Volcanic Seismology, *Annu. Rev. Earth Planet. Sci.*, *33*, 461–491, doi:10.1146/annurev.earth.33.092203.122459.

Monette, L., and M. P. Anderson (1994), Elastic and fracture properties of the two-dimensional triangular and square lattices, *Model. Simul. Mater. Sci. Eng.*, *2*, *53–66*, doi:10.1088/0965-0393/2/1/004.

Nakano, M., and H. Kumagai (2005), Waveform inversion of volcano-seismic signals assuming possible source geometries, *Geophys. Res. Lett.*, *32*, L12302, doi:10.1029/2005GL022666.

Nakano, M., H. Kumagai, and B. A. Chouet (2003), Source mechanism of long-period events at Kusatsu-Shirane Volcano, Japan, inferred from waveform inversion of the effective excitation functions, *J. Volcanol. Geotherm. Res.*, *122*(3–4), 149–164, doi:10.1016/S0377-0273(02)00499-7.

Nakano, M., H. Kumagai, B. Chouet, and P. Dawson (2007), Waveform inversion of volcano-seismic signals for an extended source, *J. Geophys. Res.*, *112*, B02306, doi:10.1029/2006JB004490.

Neuberg, J., R. Luckett, B. Baptie, and K. Olsen (2000), Models of tremor and low-frequency earthquake swarms on Montserrrat, *J. Volcanol. Geotherm. Res.*, *101*, 83–104, doi:10.1016/S0377-0273(00)00169-4.

O'Brien, G. S., and C. J. Bean (2004), A 3D discrete numerical elastic lattice method for seismic wave propagation in heterogeneous media with topography, *Geophys. Res. Lett.*, *31*, L14608, doi:10.1029/2004GL020069.

O'Brien, G. S., C. J. Bean, and H. Tapamo (2009), Dispersion analysis and computational efficiency of Elastic Lattice methods for seismic wave propagation, *Comput. Geosci.*, *35*, 1768–1775, doi:10.1016/j.cageo.2008.12.004.

Ohminato, T., B. A. Chouet, P. Dawson, and S. Kedar (1998), Waveform inversion of very long period impulsive signals associated with magmatic injection beneath Kilauea Volcano, Hawaii, *J. Geophys. Res.*, *103*, 23,839–23,862, doi:10.1029/98JB01122.

Patané, D., C. Chiarabba, O. Cocina, P. De Gori, M. Moretti, and E. Boschi (2002), Tomographic images and 3D earthquake locations of the seismic swarm preceding the 2001 Mt. Etna eruption: Evidence for a dyke intrusion, *Geophys. Res. Lett.*, *29*(10), 1497, doi:10.1029/2001GL014391.

Saccorotti, G., I. Lokmer, C. J. Bean, G. Di Grazia, and D. Patanè (2007), Analysis of sustained long-period activity at Etna Volcano, Italy, *J. Volcanol. Geotherm. Res.*, *160*, 340–354, doi:10.1016/j.jvolgeores.2006.10.008.

Schwarz, G. E. (1978), Estimating the dimension of a model, *Ann. Stat.*, *6*, 461–464, doi:10.1214/aos/1176344136.

Waite, G. P., B. A. Chouet, and P. B. Dawson (2008), Eruption dynamics at Mount St. Helens imaged from broadband seismic waveforms: Interaction of the shallow magmatic and hydrothermal systems, *J. Geophys. Res.*, *113*, B02305, doi:10.1029/2007JB005259.

C. J. Bean, I. Lokmer, and G. S. O'Brien, School of Geological Sciences, University College Dublin, Belfield, Dublin 4, Ireland. (gareth.obrien@ucd.ie)